Journal of Inorganic and Organometallic Polymers and Materials (2023) 33:462–471
https://doi.org/10.1007/s10904-022-02513-8

RESEARCH

A Trilaminar-Thermosensitive Hydrogel Catalytic Reactor Capable of Single/Tandem Catalytic Switchable Ability

Lei Pu[1] · Gang Luo[1] · Maiyong Zhu[1] · Xiaojuan Shen[1] · Wenjing Wei[2] · Songjun Li[1]

Received: 1 November 2022 / Accepted: 2 December 2022 / Published online: 14 December 2022

Abstract

The present endeavor is to develop a highly-intelligent catalytic reactor prototype which is able to autonomously adapt to the environment and provides an in-situ double-shift catalytic ability. By seeking inspiration from nature, this objective is achieved by developing a self-adaptive hydrogel catalytic reactor which held a catalytic trilaminar structure capable of reverse thermosensitive properties. With increasing temperatures, the catalytic tri-layers of this catalytic reactor would function in a sequential way (i.e., one negative temperature response layer, one support layer and one positive temperature response layer) and as a result, led to the single-tandem double-shift catalytic ability. This catalytic reactor individually presented single/tandem catalytic process at relatively low temperatures or high temperatures through the cooperative work of the three layers. In this way, this catalytic reactor showed the single-tandem controllable catalytic ability. The novel protocol not only provides a new solution to complicated catalytic processes but also inspires the further application of smart polymers in a broader spectrum of areas.

Keywords Tandem catalytic reactor · Smart hydrogels · Alterable channels

1 Introduction

Realizing controlled tandem catalysis has always been a challenge in the catalytic field, and is also a popular research area for lots of scientists [1, 2]. The use of tandem catalytic reactors can not only improve the raw material utilization and simplify the reaction process, but also reduce energy consumption. Over the years, researchers have designed and prepared a series of tandem catalytic reactors excellent in performance based on the type of thermosensitive hydrogels [3–5]. However, the lack of self-control abilities leads to decreasing efficiency on the practical applications of these thermosensitive hydrogel catalytic reactor. Therefore, it's crucial to introduce new technique strategies for developing controlled tandem catalytic reactor.

In order to develop the solutions of the self-controlled catalysis, researchers have promoted tandem catalytic reactor with new structures inspired by exploring the relationships between tissue structures in living organisms [6]. For instance, enzymes and chloroplasts catalyze reactions (typically hydrolysis and reduction) that take place in a particular way as natural reactors inspire a lot of new research [7]. In these natural reactors, a part of the tissue act as the switch of the reactors, and the other parts provide the active sites for catalytic reactions. In view of this, different catalytic reactions can take place in natural reactors with self-controlled switchable abilities.

Nowadays, functional materials have been studied to design tandem catalytic reactors, including hydrogel [8, 9],

✉ Wenjing Wei
wwei2@ed.ac.uk

✉ Songjun Li
Lsjchem@ujs.edu.cn

Lei Pu
993211690@qq.com

Gang Luo
214243387@qq.com

Maiyong Zhu
maiyongzhu@ujs.edu.cn

Xiaojuan Shen
1000004296@ujs.edu

[1] Research School of Polymeric Materials, School of Materials Science & Engineering, Jiangsu University, Zhenjiang 212013, China

[2] School of Engineering, Institute for Materials and Processes, University of Edinburgh, Robert Stevenson Road, Edinburgh EH9 3FB, Scotland, UK

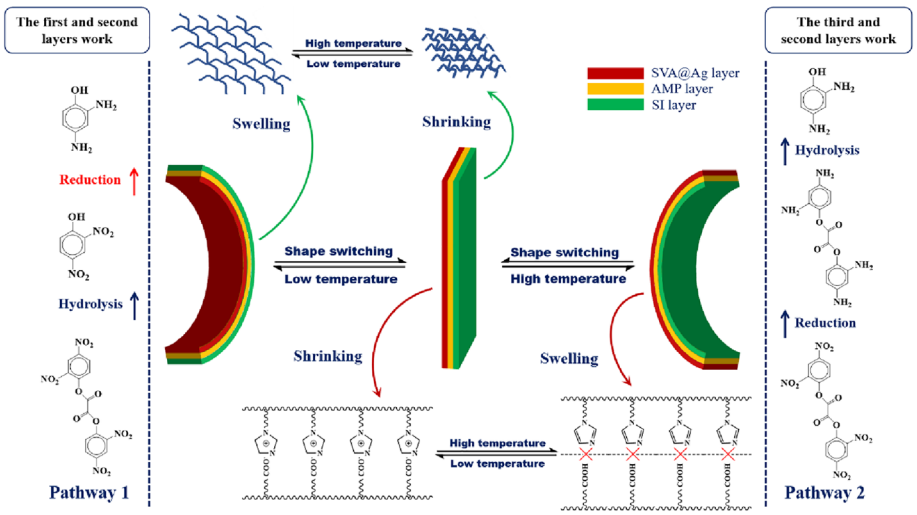

Scheme 1 Proposed mechanism for the SI-AMP-SVA@Ag catalytic reactor

Metal-Organic Frameworks [10, 11] and membranes [12, 13] and so on. Thermosensitive hydrogels are known for its technically easy method to prepare smart tandem catalytic reactors. Its temperature-responsive properties provide a switchable ability to control the reactant access in catalytic reactors. Furthermore, thermosensitive hydrogel as an excellent carrier for catalytic sites has attracted researchers' attention with different functional groups, such as hydroxyl, and acylamino, these functional groups are easy to form complexes with metal ions, which is conducive to the uniform reduction and dispersion of metal nanoparticles [14, 15]. In view of attractive features of temperature-sensitive, high physicochemical stability, low cost and simplicity in synthesis, thermosensitive hydrogels have found potential over wide areas including separation [16], catalysis [17], drug delivery [18], sensing [19] and so forth.

Inspired by this, a hydrogel tandem catalytic reactor with a self-control function was designed in this work to meet the current challenges. The catalytic reactor consists of three independent functional layers. The first layer is poly *N*-isopropylacrylamide (PNIPA) [20, 21], which acts as a switch for reactant entry into the catalytic reactor. The second layer is poly (2-acrylamide-2-methylpropanesulfonic acid) (PAMP) [22, 23], which provides acidic catalytic sites for hydrolysis. Similar to the first layer, the third layer as a switch layer consists copolymer of 1-vinylimidazole with acrylic acid [P (VIm-co-AAC)] [24] and with silver nanoparticles (Ag NPs) embedded as the active sites for reduction.

As clarified in Scheme 1, low temperature (below the LCST of PNIPA) allows the first layer to work normally cooperated with the second layer, at the same time the third layer "closed" due to the hydrophilic/hydrophobic transition of functional monomer, resulting in the substrate contacting the second layer through the first layer to catalyze hydrolysis merely. Rising temperature caused the change of the first layer from "open (hydrophilic)" to "closed (hydrophobic)", but the second layer and the third layer work normally, enabling the substrate into these layers for hydrolysis-reduction tandem reactions. Therefore, through this self-commutation, the catalytic reactor presents the changeable processes from simple catalysis to tandem catalysis [25, 26]. In this research, the thermosensitive hydrogels are using as the carriers for different kinds of catalytic reactors, which could provide a new platform for the catalytic reactor in self-controlled processes. Additionally, the combination of different functional polymers with switchable function for the complicated catalysis is a novel technology for smart catalysis.

2 Experimental Section

2.1 Materials and Reagents

All the chemicals used in the experiment are 1-ethylimidazole (VI), acrylic acid (AAc), 2-acrylamido-2-methylpropanesulfonic acid (AMPS), *N*-isopropylacrylamide (NIPAM), silver nitrate ($AgNO_3$), AIBN, N, *N*'-methylene bisacrylamide (MBA), dimethyl sulfoxide (DMSO), sodium borohydride ($NaBH_4$), polystyrene, ethanol and acetic acid. The chemicals used were of analytic grade and used as received from Sigma-Aldrich, unless otherwise noted. Ultrapure water was adopted in all experiments.

2.2 Catalytic Reactors Preparation

2.2.1 Preparation of the P(VIm-co-AAc) Layer

The preparation method of the catalyst in this paper was based on other research content [27]. In details, VI (1.88 g;

0.02 mol), AAc (1.44 g; 0.02 mol), $AgNO_3$ (0.1 g), AIBN (0.06 g), MBA (0.2 g), were dissolved in DMSO (10 mL). After being dispersed with sonication and deoxygenated by nitrogen, the mixture system was kept at 70 °C for 3 h to polymerize the first layer (P(VIm-co-AAc) layer). The encapsulated Ag ions were subsequently reduced with an excess of sodium borohydride. Then the product was washed with deionized water and placed overnight until dry.

2.2.2 Preparation of the PAMP/P(VIm-co-AAc) Layers

Following this, the P(VIm-co-AAc) layer was exposed to the solution intended for the preparation of the next layer, in which AMPS (3.1 g; 0.015 mol), AIBN (0.06 g) and MBA (0.12 g) were dissolved in DMSO (10 mL). After deoxygenation, polymerization was then performed at 70 °C for 3 h to synthesize the middle layer (PAMP layer).

2.2.3 Preparation of the PNIPA/PAMP/P(VIm-co-AAc) Catalytic Reactor

Finally, NIPAM (3.36 g; 0.03 mol), AIBN (0.06 g) and MBA (0.134 g) were dissolved in DMSO (10 mL). After deoxygenation, the prepared P(VIm-co-AAc) /PAMP was contacted with the solution and reacted at 70 ℃ for 3 h to obtain the PNIPA layer. In this way, the three-layer catalytic reactor was prepared.

The trilaminar structure hydrogel catalytic reactor was named "SI-AMP-SVA@Ag". "S" means switchable ability, "I" is the PNIPA, "AMP" represents PAMP, "V" and "A" represent the VI and PAAc that make up the third layer, where "Ag" means the Ag NPs.

Two control catalytic reactors were prepared in similar conditions but either without thermo-sensitive components or metal nanoparticles (named "NS-AMP-SVA@Ag", and "SI-AMP-NS"; herein, "N" means no-switchable properties). Comparing with the novel catalytic reactor, the sensitive layer in NS-AMP-SVA@Ag was substituted with polystyrene (named "PS") that a strong-hydrophobic and non-responsive monomer.

2.3 Materials Characterization

Sample powder of each layer was scraped and grinded from the dried catalytic reactors and the Fourier transform infrared spectrum (FTIR) of sample powder was collected through the MX-1E apparatus. A MIRA3-XMU apparatus was used to collect the energy-dispersive spectra (EDS). Microstructure and size of metal nanoparticles were observed by a transmission electron microscope (TEM, JEM-2100). The Shimadzu UV-2600 spectrophotometer (Japan) was used to detect the surface plasma resonance spectra (SPR). A digital camera was used to record the shape change behaviors of catalytic reactor in rising temperature.

2.4 Thermosensitive Transition

The thermo-responsive properties of the three layers in catalytic reactor were separately analyzed by a dynamic light scattering (DLS) (Bettersize-2450, China) [28]. The sample powder scraped from three layers of catalytic reactor should be dispersed in water for 20 h for balancing. The upper liquid was used for the test.

2.5 Catalytic Properties

DNPO was dissolved in 25 mL of PBS (pH 7.0) with an initial concentration of 0.25 μmol mL^{-1} (The dosage of $NaBH_4$ was 0.01 g, fourfold as compared with DNPO). The dosage of the catalytic reactor was 15 mg mL^{-1}. Placing a 50 ml beaker with the solution to be tested in a constant temperature oscillator to heat for specified temperature and vibrate at 160 r/min. Taking the solution every 10 min and record the absorbance. The catalytic activity of catalytic reactors was determined from the average of triple runs, using spectrophotometry by the UV-2700 spectrophotometer (Japan) to monitor the change of the absorbance peak of the DNPO during the catalytic process [29, 30]. The activity of hydrolysis of DNPO was deducted on the same conditions without catalytic reactors from the whole system to avoid the influence of self-hydrolysis behavior on the catalytic efficiency. The conversion (α) of reactant DNPO was defined as the amount of DNPO that was catalyzed for DNP or DAPO in solution, and calculated by Eq. (1):

$$\partial = \frac{C_0 - C_t}{C_0} \times 100\% \quad (1)$$

where C_0 and C_t denote the absorbance of DNPO initial concentrations and the concentrations of t min in UV–vis spectra, respectively.

2.6 Desorption electrochemistry

The interactions between the catalytic reactors and substrates were characterized by desorption electrochemistry [31, 32]. The catalytic reactors (10 mg) which preabsorbed with ~2 mmol of substrate were placed in the electrochemical cells encircled by a diffusion-eliminating sonication apparatus (supporting electrolyte: 10 mL PBS; pH 7.0). The desorbing behavior of the absorbed substrate was monitored by using an electrochemical workstation equipped with a conventional three-electrode configuration (Au-plate working electrode, Pt-wire counter electrode and calomel electrode reference electrode) and circularly scanning the system until a stable

desorption profile was reached (scanning range: − 0.6 ~ 0.6 V; scanning rate: 1 mV s^{-1}).

3 Results and Discussion

3.1 Analysis of the FTIR Spectrum

Further investigation of the different polymer components in the three layers of the catalytic reactor was carried out through the FTIR analysis. In Fig. 1a, three main bands (3100–3700, 1600–1800 and 1000–1500 cm-1), respectively related to C–H/N–H, C = O and C–C/C–N bonds of the stretching vibration [33, 34]. As shown in Fig. 1b, S = O bonds (1045 cm^{-1}) in the sulfonic acid groups appear in the PAMP layer merely, confirming the existence of the PAMPS. Meanwhile, the participating of PNIPAM was confirmed by the presence of the associated peak of the amide II band at 1639 cm^{-1} in the third layer of Si-AMP-SVA@Ag (Fig. 1c). The appearance of characteristic peaks of polystyrene indicates included the bending vibration peak of benzene ring (1601, 1492 and 1451 cm^{-1}) and the out-of-plane bending vibration of C–H (756, 689 cm^{-1}) band that the temperature-sensitive components in NS-AMP-SVA@Ag and Si-AMP-NS were replaced by styrene successfully (Fig. 1a and c). For the identical layers in the control groups, the spectra are comparable due to the same compositions involved in the catalyst. For the identical layers in the control groups, the spectra are comparable due to the same compositions involved in the catalytic reactor [35].

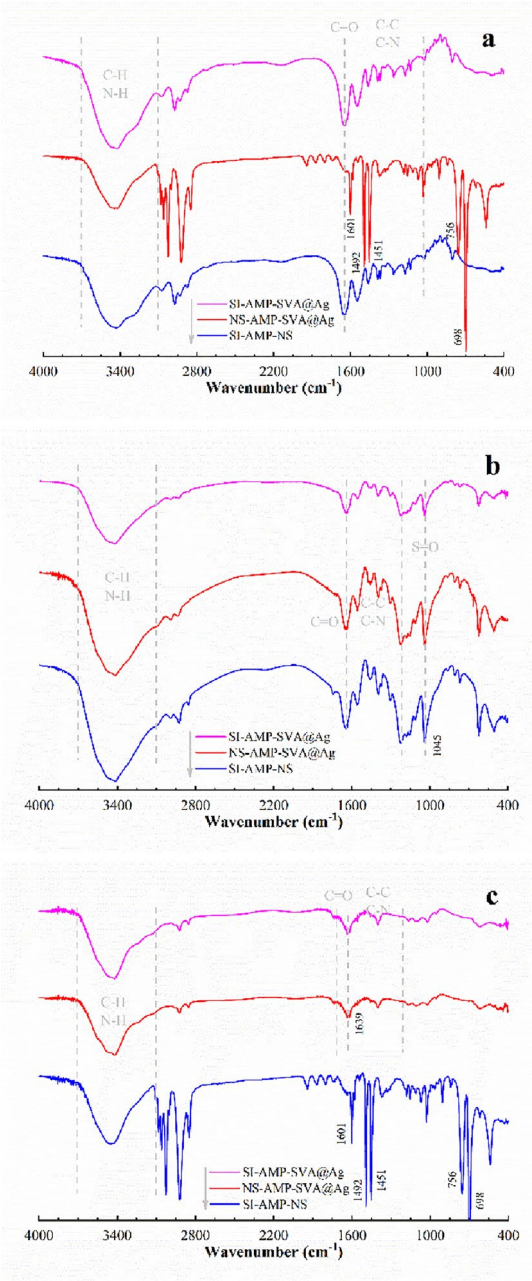

Fig.1 FTIR spectra of the three layers in the prepared catalytic reactors (**a** the first layer; **b** the second layer; **c** the third layer)

3.2 Analysis of Composition and Morphology

Both layers of SI-AMP-SVA@Ag contain C, N and O elements. Herein, the content of S and Ag in the catalytic reactor was 14.97wt% and 3.82wt% by EDS analysis in Fig. 2 respectively.

Figure 3 presents the TEM images, displaying the metal nanoparticles with a size of ~ 5 nm were encapsulated in SI-AMP-SVA@Ag and NS-AMP-SVA@Ag. The TEM image of SI-AMP-NS lacks black particles, indicating the sample are prepared without metal nanoparticles. The existence of Ag nanoparticles is ascertained by the tests of SPR (Fig. 4). Different kinds of metal nanoparticles have different peak positions in SPR spectra. The characteristic peaks of Ag nanoparticles appear at 415 nm for SI-AMP-SVA@Ag and NS-AMP-SVA@Ag thus proving that Ag + has been successfully reduced in polymer catalytic reactors [36].

3.3 Self-Controllable Ability and Shape Switchable Behaviors

The dynamic radius of the samples scraped from the thermosensitive layers is studied as a function of temperature to further address the thermosensitive properties. By comparing the non-responsive layers in the control groups, the shape switchable contribution of thermo-responsive layers in SI-AMP-SVA@Ag is reflected from the relative change of the dynamic radius upon changing temperatures. As shown in Fig. 5, in contrast to the non-responsive AMP and NS layers which is non-responsive toward temperature, the dynamic radius (Rd) of both the thermosensitive layers shows significant temperature dependence. With the increase

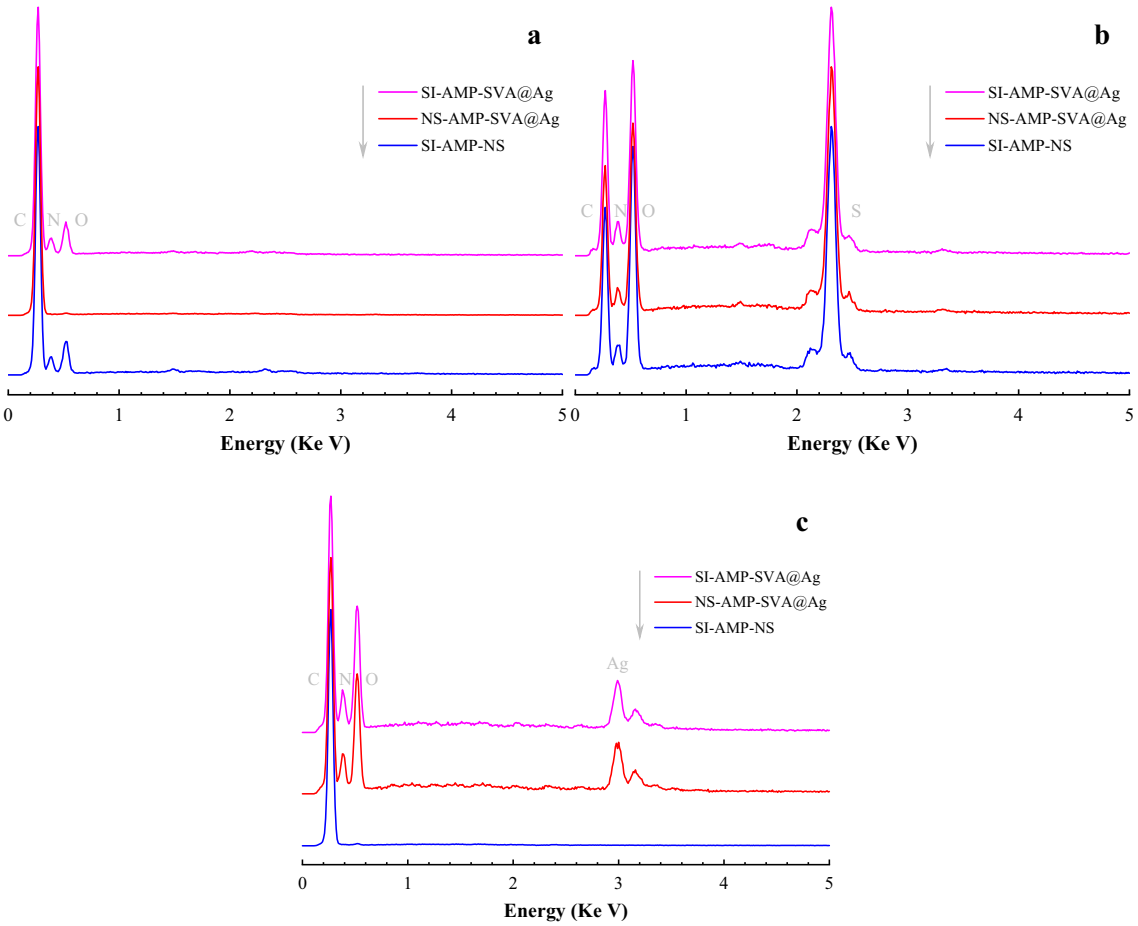

Fig. 2 EDS spectra of the prepared catalytic reactors (**a** the first layer; **b** the second layer; **c** the third layer)

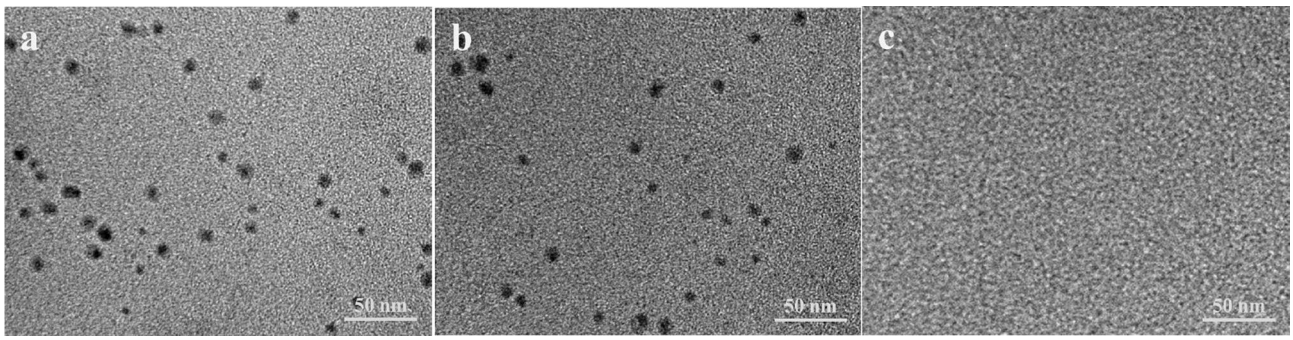

Fig. 3 TEM images of the Ag nanoparticles encapsulated in these catalytic reactors (**a** SI-AMP-SVA@Ag; **b** NS-AMP-SVA@Ag; **c** SI-AMP-NS)

of temperature, the dynamic radius of the SI layer decrease and the major change appears at 32 ℃. Below 32 °C, the SI layer shows relatively a bigger radius; while above it, the dynamic radius of the SI layer dramatically decreases to a level almost comparable to that of the NS layer which runs on the closed networks. The mutation of the SI layer is due to the hydrophilic/hydrophobic transition of PNIPA. The thermosensitive properties of the SVA@Ag layer show a dramatic increase at 40 °C. When the temperature is low, the interactions between hydrogen bonds of the SVA@Ag

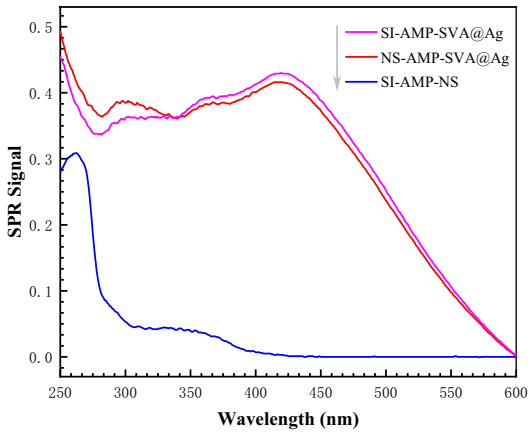

Fig. 4 SPR spectra of the prepared catalytic reactors

layer leads to a closed access. However, with the temperature rising above 40 °C, the dynamic radius of the SVA@Ag layer dramatically increases to allow reactant contacting Ag NPs. In essence, this behavior was due to the generation and destruction of electrostatic interactions between carboxyl and imidazole groups. These results indicates that the changeable shape behavior in the catalytic reactor is due to the cooperation between the two thermosensitive layers. In this way, different pathways are formed in two temperature ranges (below 32 °C and above 40 °C) to promote single/tandem switchable catalysis reactions, respectively.

The shape switchable behaviors of the catalytic reactor with different temperatures are shown in Fig. 6. In water, the catalytic reactor appeared to be concave to the left at 20 °C, following flat at 35 °C and it changed to concave to the right when the temperature was 50 °C. The catalytic reactor could switch curve and flat shapes upon changing temperature and the shape switchable behaviors were reversible.

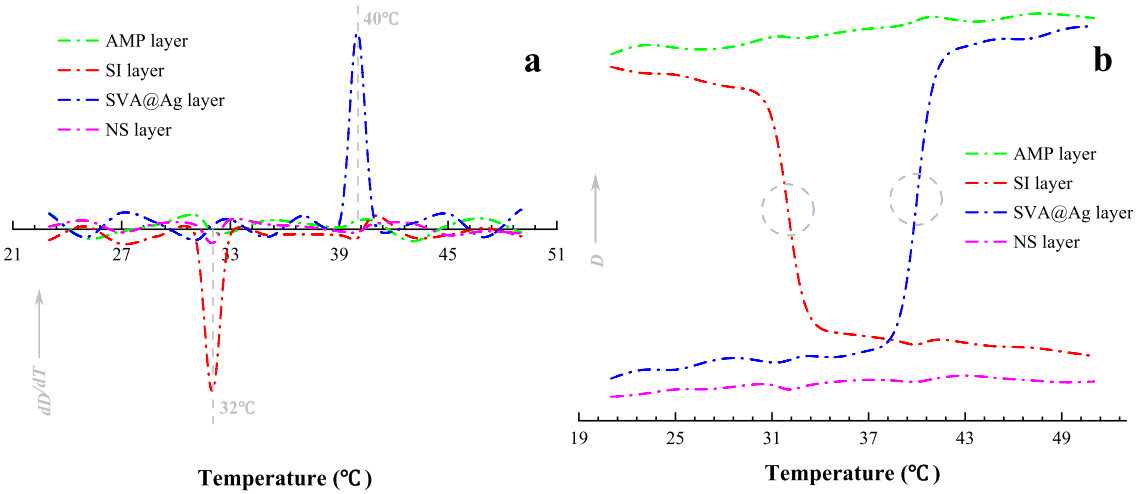

Fig. 5 DLS spectra with dynamic diameter changing as a function of temperature (**a** Differential; **b** Normal)

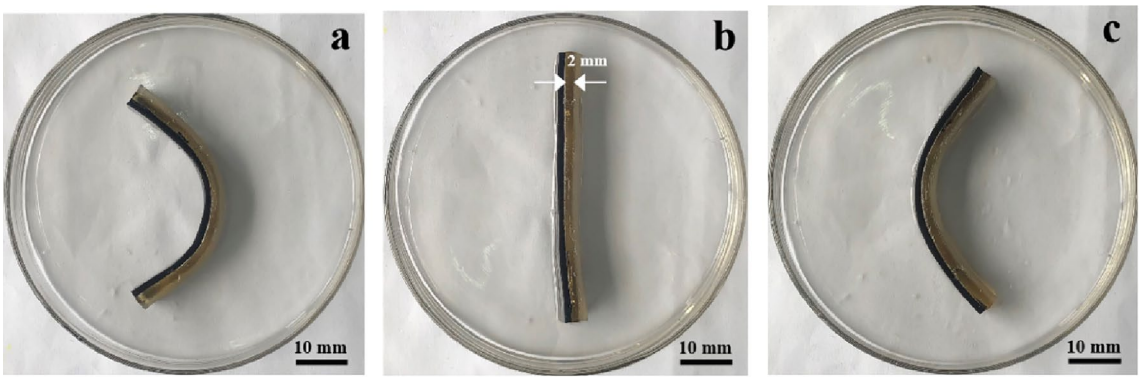

Fig. 6 Alterable morphology of SI-AMP-SVA@Ag (**a** 20 ℃; **b** 35 ℃; **c** 50 ℃)

3.4 Single/Tandem Switchable Catalytic Ability

Single/tandem catalytic reactions (i.e., reductive hydrolysis and hydrolysis reactions) need to be carried out at specific temperatures, so three temperatures (20 ℃, 35 ℃ and 50 ℃) are selected to test the catalytic performance. Firstly, the hydrolysis performance of the catalytic reactors is tested at 20 ℃ and 35 ℃ without sodium borohydride (a reducing agent for catalytic reduction). As shown in Fig. 7, at 20 °C, SI-AMP-SVA@Ag and SI-ANP-NS show higher catalytic activity of hydrolysis than the NS-AMP-SVA@Ag which the strong hydrophobicity of the PS layer prevents substrate to enter the catalytic reactor. Because of the hydrophilic/hydrophobic transition of the PNIPA, at 40 °C, catalytic reactors with switchable SI layers exhibits low hydrolysis catalytic efficiency. Then the tandem catalytic performance of the SI-AMP-SVA@Ag and controls are tested at 50 ℃ with sodium borohydride. All catalytic reactors show active tandem catalytic performance, because the electrostatic interactions between imidazole and carboxyl groups are destroyed and the substrate could enter catalytic reactors. By comparing the catalytic efficiency (Fig. S1a, 70%) of system that merely adding DNPO and reducing agent in the same time, the addition of Si-AMP-SVA@Ag could improve the catalytic efficiency by 32.3%. In this way, SI-AMP-SVA@Ag exhibits characteristic single/tandem catalytic processes.

To study the controllable tandem catalytic ability of the SI-AMP-SVA@Ag, the tests are carried out at 20 ℃ firstly. In this condition, in Fig. 8a, SI-AMP-SVA@Ag and SI-AMP-NS with opened first layer show the peak of DNPO (360 nm) decreasing and DNP (260 nm) increasing, exhibiting that the DNPO was hydrolyzed to DNP. The closed channel in the first layer of NS-AMP-SVA@Ag forbad DNPO to contact the acid active site to catalyze hydrolysis. While at 35 °C (Fig. 8b), the performance of all catalytic reactors decreases because it lacks the channels that allow substrate to contact catalytic sites. After reducing DNPO to DAPO (301 nm) by Ag nanoparticles, the intermediate product DAPO is hydrolyzed to DAP (285 nm) by acidic sites at 50 °C (Fig. 8c). The catalysis tests show that the trilaminar catalytic reactor SI-AMP-SVA@Ag conduct the single/tandem catalytic reactions with increasing temperature, achieving switchable catalytic performance toward different temperature zones.

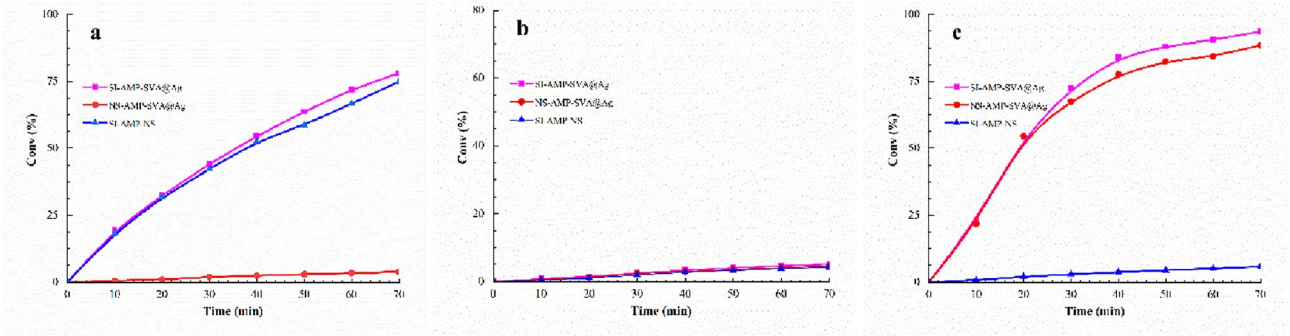

Fig. 7 Catalytic activities of the prepared catalytic reactors (**a** 20 ℃; **b** 35 ℃; **c** 50 ℃)

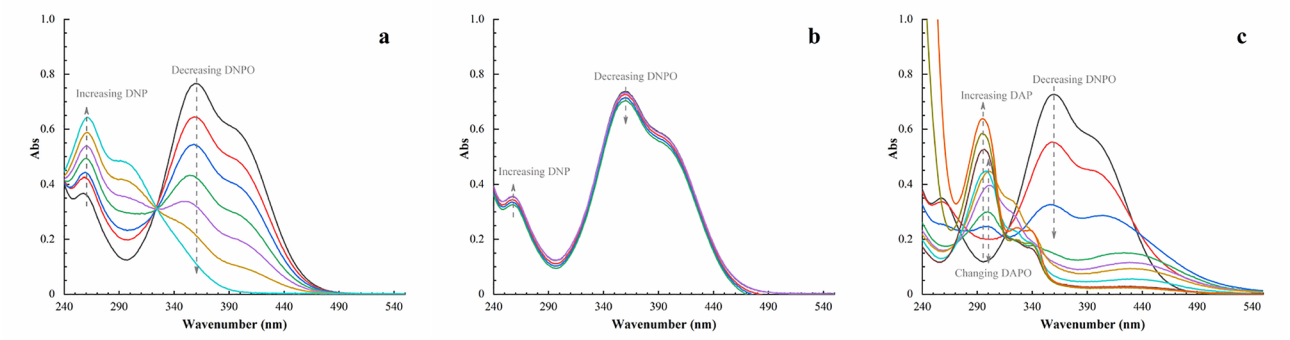

Fig. 8 The changing UV spectrum of DNPO with sodium borohydride at catalytic reactors (**a** SI-AMP-SVA@Ag / SI-AMP-NS at 20 ℃; **b** SI-AMP-SVA@Ag at 35 ℃; NS-AMP-SVA@Ag at 20 ℃ and 35 ℃; SI-AMP-NS at 35℃ and 50℃; **c** SI-AMP-SVA@Ag / NS-AMP-SVA@Ag at 50 ℃)

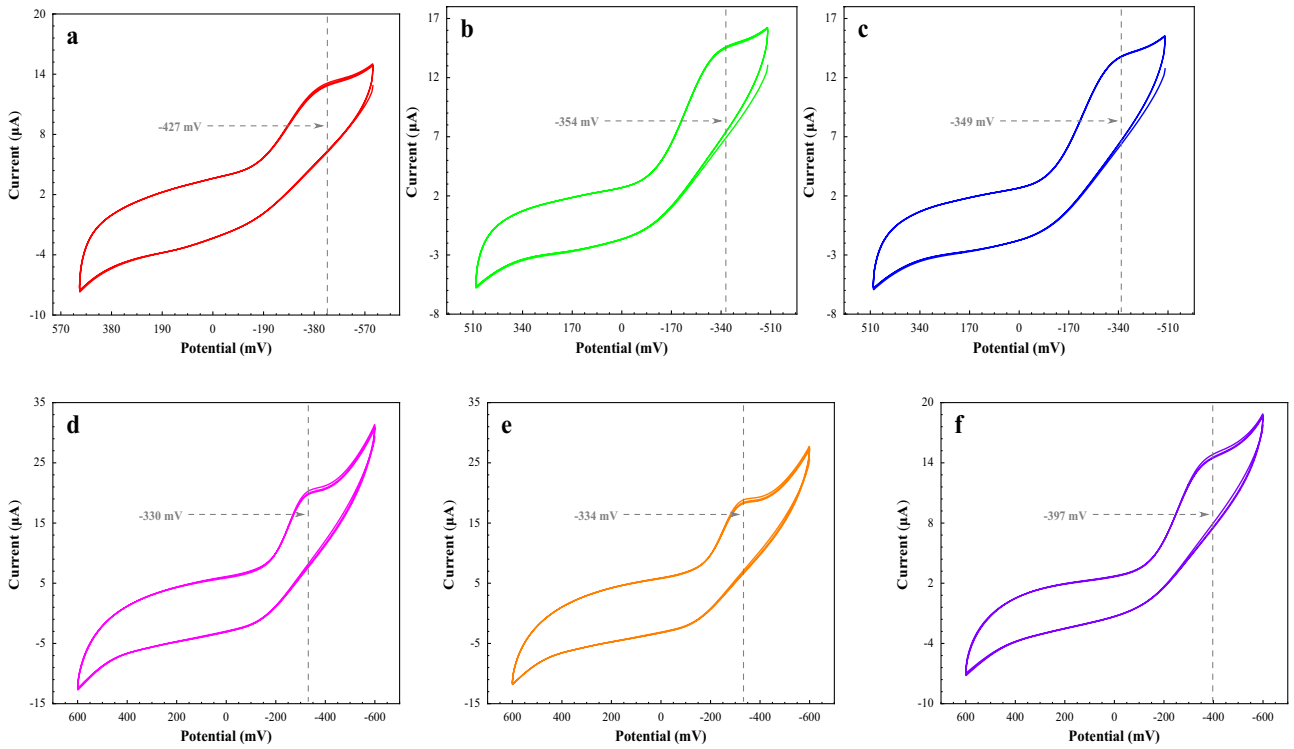

Fig. 9 Desorption-reduction profiles with DNPO desorbing from SI-AMP-SVA@Ag (**a**, **b**, **c**: SI layer at 20 ℃/35 ℃/50 ℃; **d**, **e**, **f**: SVA@Ag layer at 20 ℃/35 ℃/50 ℃)

Table 1 Desorption-reduction potentials with substrates desorbing from all layers in the catalytic reactors

Layers	Reduction potential (mV)			Delta 1	Delta 2
	20 ℃	35 ℃	50 ℃	20 ℃→35 ℃	35 ℃→50 ℃
SI layer	− 427	− 354	− 349	73	5
SVA@Ag layer	− 330	− 334	− 397	− 4	− 63
AMP layer	− 287	− 282	− 278	5	4
NS layer	− 303	− 301	− 298	2	3

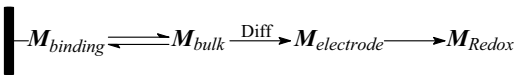

Scheme 2 Schematic presentation of the desorbing electrochemical-process with binding M

3.5 Dynamic Binding and Controlled Entrance

The self-actuating switchable properties of the two layers in the proposed catalytic reactors are further investigated by desorption electrochemistry (Fig. 9; Table 1). Normally, the larger potential for substrate releasing depicts the stronger interactions engaging in the dynamic release process [37, 38]. The detailed theory, as outlined in Scheme 2, has been described elsewhere [39]. The binding substrate in the electrochemical system would normally involve desorption, diffusion to the surface of electrodes, and the terminal redox process. Once the diffusion is eradicated with sonication, the desorbing behavior of the binding substrate was hence directly correlated to the change of the redox potential.

To track the triple-shift switchable properties, 20 °C, 35 °C and 50 °C are selected again for a contrastive study. As shown in Fig. 9, the desorption-reduction potential of the first layer of SI-AMP-SVA@Ag shifts from − 427 to − 354 mV from 20 °C to 35 °C and further shifted to − 349 mV at 50 °C. The significant change at 35 °C results from the closed network of the first layer. As a result of the channel in the third layer gradually opening, from 35 to 50 °C, the desorption reduction potential of SI-AMP-SVA@Ag dramatically changes from − 334 mV to − 397 mV.

These results indicate that there are temperature response channels in the polymer catalytic reactor. The changes in desorption-reduction potential are further shown in Table 1. Electrochemical tests are carried out on both the experimental and controls. For the PAMP and NS layers with no thermal sensitivity, the interactions between catalytic reactor

and substrate are almost unaffected by temperature. On the contrary, the change of temperature can cause the abrupt change of desorption potential of the SI layer and SVA@Ag layer that temperature change caused phase change. The desorbing performance of the controls further proves the temperature-responsive properties of trilaminar layers catalytic reactor SI-AMP-SVA@Ag. It can be concluded that the temperature sensitive transition between the PNIPA layer and the P(VIm-co-AAC) layer is one of the reasons for the simple/tandem catalytic reactions.

4 Conclusion

In this research, a novel tandem hydrogel catalytic reactor was prepared, which provides a method to address the self-controlled challenges of complicated reactions in the current catalytic fields. This catalytic reactor with a trilaminar structure consists of a negative temperature-sensitive layer, a support layer containing acid catalytic sites and a positive temperature-sensitive layer with Ag nanoparticles. The inverse responsiveness and alternating coupling from the two temperature-sensitive layers result in the shape switchable behaviors, thereby enabling the catalytic reactors to perform different single/tandem changeable reactions at different temperatures. Thus, the catalytic reactor shows self-controlled catalytic capability. These impressive properties make SI-AMP-SVA@Ag hydrogel catalytic reactors more promising for complex practical applications.

Supplementary Information The online version contains supplementary material available at https://doi.org/10.1007/s10904-022-02513-8.

Author contributions LP: Writing-Original Draft; Formal analysisGL: Investigation; Methodology.MZ: Writing – Review & EditingXS: Writing – Review & EditingWW: Formal analysis; Writing – Review & EditingSL: Resources; Supervision; Project administration.

Funding The authors have not disclosed any funding.

Declarations

Conflict of interest The authors declare no conflict of interest concerning in the present study.

References

1. Yu. Zhao, G. Yang, J. Pan et al., Tandem catalytic indolization/enantioconvergent substitution of alcohols via borrowing hydrogen to access tricyclic indoles. Angew. Chem. Int. Ed. **60**, 20689–20694 (2021)
2. P. Xiao, Wu. Shuping, X. Shen et al., Smart tandem catalyst developed with sundew's predation strategy, capable of catching, decomposing and assimilating preys. ChemCatChem **10**, 5231–5241 (2018)
3. Y. Tan, Di. Wang, Xu. Huaxiu et al., A fast, reversible, and robust gradient nanocomposite hydrogel actuator with water-promoted thermal response. Macromol. Rapid Commun. **39**, 1700863 (2018)
4. P. Ni, S.Y. RenpengLi et al., Lactobionic acid-modified chitosan thermosensitive hydrogels that lift lesions and promote repair in endoscopic submucosal dissection. Carbohyd. Polym. **263**, 118001–118001 (2021)
5. B.K. Bozoğlan, O. Duman, S. Tunç, Preparation and characterization of thermosensitive chitosan/carboxymethylcellulose/scleroglucan nanocomposite hydrogels. Int. J. Biol. Macromol. **162**, 781–797 (2020)
6. M. Omidvar, J. Zdarta, S.B. Sigurdardóttir et al., Mimicking natural strategies to create multi-environment enzymatic reactors: From natural cell compartments to artificial polyelectrolyte reactors. Biotechnol. Adv. **54**, 107798 (2021)
7. P. Zhu, L. Wang, F. Stewart et al., Direct conversion of natural gases in solid oxide cells: A mini-review. Electrochem. Commun. **128**, 107068 (2021)
8. W. Wei, P. Xiao, V.K. Thakur et al., Smart bilayer polymer reactor with cascade/non-cascade switching catalyst characteristics. Mat. Today Chem. **17**, 100279 (2020)
9. D. Parida, E. Moreau, R. Nazir et al., Smart hydrogel-microsphere embedded silver nanoparticle catalyst with high activity and selectivity for the reduction of 4-nitrophenol and azo dyes. J. Hazard. Mater. **416**, 126237–126237 (2021)
10. Y. Zhang, C. Huang, L. Mi, Metal–organic frameworks as acid-and/or base-functionalized catalysts for tandem reactions. Dalton Trans. **49**, 14723–14730 (2020)
11. Hu. Yanjing, J. Zhang, H. Huo et al., One-pot synthesis of bimetallic metal-organic frameworks (MOFs) as acid-base bifunctional catalysts for tandem reaction. Catal. Sci. Technol. **10**, 315–322 (2019)
12. S. Schlüter, K.U. Künnemann, M. Freis et al., Continuous co-product separation by organic solvent nanofiltration for the hydroaminomethylation in a thermomorphic multiphase system. Chem. Eng. J. **409**, 128219 (2021)
13. C. Huang, K. Zhu, Lu. Guizhen et al., Oriented assembly of copper metal-organic frameworks membranes as tandem catalysts to enhance C–H hydroxyalkynylation reactions with regiocontrol. CrystEngComm **22**, 802–810 (2019)
14. H. Zhu, Z. Li, J. Yang, A novel composite hydrogel for adsorption and photocatalytic degradation of bisphenol A by visible light irradiation. Chem. Eng. J. **334**, 1679–1690 (2018)
15. Z. Zhao, Z. Xiao, C. Qin et al., Sandwich-like N-C/Cu/N-C porous beads derived from alginate with enhanced catalytic activity and excellent recyclability for 4-nitrophenol reduction. Ind. Crops Prod. **164**, 113413 (2021)
16. S. Dong, S. Li, Y. Hao et al., Hydroxybutyl starch-based thermosensitive hydrogel for protein separation. Int. J. Biol. Macromol. **134**, 165–171 (2019)
17. Z. Xiao, Y. Tan, J. Ma et al., Fast swelling behaviors of thermosensitive poly[N-isopropylacrylamideco-methacryloxyethyltrimethyl ammonium chloride]/Na_2WO_4 cationic composite hydrogels. J. Appl. Polym. Sci. **135**, 46375–46375 (2018)

18. J. Tucker Luke, S. Grant Christine, A. Gautreaux Malley et al., Physicochemical and antimicrobial properties of thermosensitive chitosan hydrogel loaded with fosfomycin. Mar. Drugs **19**, 144–144 (2021)
19. Fu. Jiahui Sun, H.H. Zhou et al., Photocontrolled thermosensitive electrochemiluminescence hydrogel for isocarbophos detection. Anal. Chem. **92**, 6136–6143 (2020)
20. Pu. Lei, M. Zhu, X. Shen et al., Stomata-inspired smart bilayer catalyst with the dual-responsive ability, capable of single/tandem catalysis. Polymer **234**, 124238 (2021)
21. N. Pentela, V. Gayathri, D. Samanta, N-heterocyclic carbene bearing thermoresponsive poly(NIPAM) supported palladium (II) complex: Synthetic strategy and application. J. Organomet. Chem. **913**, 121196–121196 (2020)
22. J.C. AbdulHaleem, X. Guo et al., Hybrid cryogels composed of P(NIPAM-co-AMPS) and metal nanoparticles for rapid reduction of p-nitrophenol. Polymer **193**, 122352–122352 (2020)
23. D. Sinem, O. Hava, Ag(0) nanocatalyst stabilized with networks of p(SPA-co-AMPS) for the hydrogen generation process from ethylenediamine bisborane hydrolysis. Int. J. Hydrogen Energy **45**, 17649–17661 (2020)
24. V.V. Annenkov, E.N. Danilovtseva, H. Tenhu et al., Copolymers of 1-vinylimidazole and (meth)acrylic acid: Synthesis and polyelectrolyte properties. Eur. Polymer J. **40**, 1027–1032 (2003)
25. X. Zhang, Ou. Xiaojian, J. Zhang et al., Smart ion imprinted polymer for selective adsorption of Ru(III) and simultaneously waste sample being transformed as a catalyst. J. Hazard. Mater. **417**, 126072 (2021)
26. C. Tian, S. Han, J. Zhu et al., In situ growth of multifunctional porous organic polymer nanofilms with molecular sieving and catalytic abilities. Chem. Eng. J. **427**, 130978 (2022)
27. W. Wei, V.K. Thakur, Y.M. John Chew et al., Towards next generation "smart" tandem catalysts with sandwiched mussel-inspired layer switch. Mat. Today Chem. **17**, 100286 (2020)
28. T. Kureha, H. Minato, D. Suzuki et al., Concentration dependence of the dynamics of microgel suspensions investigated by dynamic light scattering. Soft Matter **15**, 5390–5399 (2019)
29. M. Ma, Y. Yang, W. Li et al., Gold nanoparticles supported by amino groups on the surface of magnetite microspheres for the catalytic reduction of 4-nitrophenol. J. Mater. Sci. **54**, 323–334 (2019)
30. S. Li, Y. Ge, A. Tiwari et al., 'On/off'-switchable catalysis by a smart enzyme-like imprinted polymer. J. Catal. **278**, 173–180 (2011)
31. R. Luo, M. Zhu, X. Shen et al., Polymer catalyst with self-assembled hierarchical access for sortable catalysis. J. Catal. **331**, 49–56 (2015)
32. S. Back, Y. Jung, On the mechanism of electrochemical ammonia synthesis on the Ru catalyst. Phys. Chem. Chem. Phys. **18**, 9161–9166 (2016)
33. C. Yan, P.L. Kramer, R. Yuan et al., Water dynamics in polyacrylamide hydrogels. J. Am. Chem. Soc. **140**, 9466–9477 (2018)
34. C. Shan, L. Wang, Z. Li et al., Graphene oxide enhanced polyacrylamide-alginate aerogels catalysts. Carbohyd. Polym. **203**, 19–25 (2019)
35. J. Wang, Y. Xianghu, C. Wang et al., PAMPS/MMT composite hydrogel electrolyte for solid-state supercapacitors. J. Alloy. Compd. **709**, 596–601 (2017)
36. F.K. Alsammarraie, P.Z. WeiWang et al., Green synthesis of silver nanoparticles using turmeric extracts and investigation of their antibacterial activities. Colloids Surf., B **171**, 398–405 (2018)
37. Z. Xia, W. Wei, M. Zhu et al., Artificial reactor containing polymeric bilayer architectures for the formation of self-controlled tandem catalytic-ability. Express Polym. Lett. **14**, 12–25 (2020)
38. J. Huang, R. Buonsanti, Colloidal nanocrystals as heterogeneous catalysts for electrochemical CO_2 conversion. Chem. Mater. **31**, 13–25 (2018)
39. L. Hua, M. Xie, Y. Jian et al., Multiple-responsive and amphibious hydrogel actuator based on asymmetric UCST-type volume phase transition. ACS Appl. Mater. Interfaces. **11**, 43641–43648 (2019)